DIBOSON PHYSICS AT THE TEVATRON

JADRANKA SEKARIC
for the CDF and DØ Collaborations
Department of Physics and Astronomy, 1082 Malott, 1251 Wescoe Hall Drive, University of Kansas, Lawrence, Kansas 66045, USA

We present recent measurements of diboson production at the Tevatron Collider at $\sqrt{s}$ = 1.96 TeV, analyzing fully leptonic and semileptonic final states in data collected by the CDF and DØ detectors between 2002 and 2011. The analyzed final states in $W\gamma$, $Z\gamma$, WW, WZ and ZZ production are of significant importance for testing the electroweak sector of the Standard Model and they are directly relevant to searches for a low mass Higgs boson and physics beyond the Standard Model.

1 Introduction

Precision measurements of diboson processes play an important role in electroweak physics and searches for new physics which may exist at some high energy scale Λ. In the presence of new physics, observables such as production cross sections, the trilinear gauge boson couplings (TGCs) [1], and various kinematic distributions, are expected to deviate from their Standard Model (SM) predictions. The charged TGCs present in WW, WZ and $W\gamma$ production are Δg_1^V, $\Delta\kappa_V$ and λ_V ($V = Z$ or γ) where Δ represents the deviation from the SM prediction. In the SM, $\Delta g_1^V = \Delta\kappa_V = \lambda_V = 0$. The neutral TGCs h_i^V ($i = 3, 4$), studied in $Z\gamma$ production, are not allowed in the SM at tree-level, and their values are predicted to be zero. Dibosons also represent an important background in production of the top quark, Higgs boson(s) and exotic particles. Thus, precise knowledge of diboson processes and their proper modeling is important for current and future studies.

2 Diboson Production

2.1 $W\gamma$ Production

Due to negative interference among the tree-level diagrams, the amplitude for SM $W\gamma$ production is expected to be zero around $cos\theta$ = -0.3 (θ is an opening angle between incoming quark and outgoing W boson) known as the Radiation Amplitude Zero (RAZ). The effect is also evident in the charge-signed lepton-photon rapidity difference as a dip around -0.3, shown in Fig.1. The data analyzed by the DØ Collaboration correspond to 4.2 fb^{-1}. An isolated electron (muon) is required to be in the region $|\eta_e| < 1.1$ or $1.5 < |\eta_e| < 2.5$ ($|\eta_\mu| < 1.6$) with $E_T > 25$ GeV (20 GeV). In both channels, the photon must be detected in $|\eta_\gamma| < 1.1$ or $1.5 < |\eta_\gamma| < 2.5$ with $E_T > 15$ GeV and separated from the lepton by $\Delta R_{l\gamma} > 0.7$ where $\Delta R = \sqrt{(\Delta\phi)^2 + (\Delta\eta)^2}$ [2]. The event is required to have $\not\!\!E_T > 20$ GeV and a three-body transverse mass, $M_{l\nu\gamma}$, greater

than 110 GeV. According to the number of selected signal events the measured cross section corresponds to $\sigma_{W\gamma} \times$ BR$(W \to l\nu) = 7.6 \pm 0.4$ (stat) $\pm$ 0.6 (syst) pb which is in agreement with the SM prediction of 7.6 $\pm$ 0.2 pb. The photon E_T spectra shown in Fig. 2 were used to set one-dimensional 95% C.L. limits on anomalous TGCs of -0.4 $< \Delta\kappa_\gamma <$ 0.4 and -0.08 $< \Delta\lambda_\gamma <$ 0.07 for Λ = 2 TeV [3].

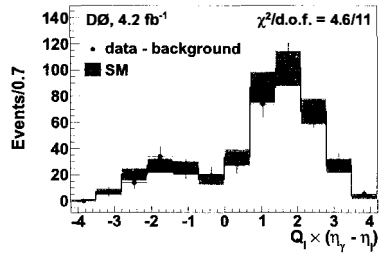

Figure 1: The charge-signed photon-lepton rapidity difference for background-subtracted data and $W\gamma$ MC prediction.

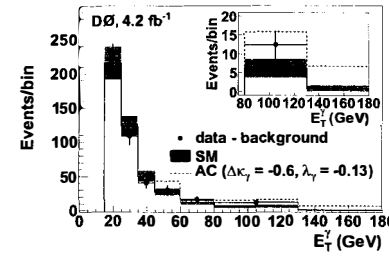

Figure 2: Photon E_T spectra for observed and predicted $W\gamma$ events and the expected distribution in the presence of anomalous TGCs.

2.2 $Z\gamma$ Production

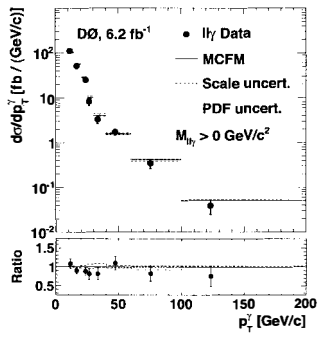

Figure 3: Unfolded $d\sigma/dp_T$ distribution for $ll\gamma$ events compared to MCFM NLO prediction.

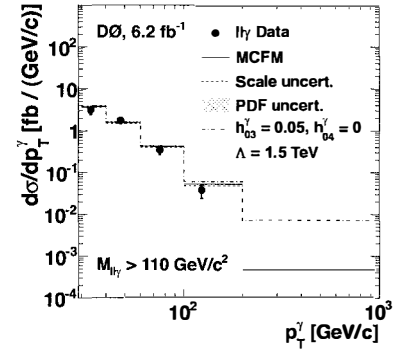

Figure 4: Unfolded $d\sigma/dp_T$ distribution for $ll\gamma$ events used to set the 95% C.L. limits on TGCs.

The $Z\gamma$ events are reconstructed from 6.2 fb^{-1} of DØ data using the $ll\gamma$ final states ($l = e, \mu$) [4]. In the electron channel at least one electron is required to have $E_T > 25$ GeV (a second electron $E_T > 15$ GeV) and must be reconstructed within $|\eta_e| < 1.1$. In the muon channel one muon is required to have $p_T > 20$ GeV and the second must have $p_T > 15$ GeV. In both channels an event is selected if the invariant mass of the ll pair is larger than 60 GeV. A photon candidate with $E_T > 10$ GeV is reconstructed within $|\eta_\gamma| < 1.1$, separated from the lepton by $\Delta R_{l\gamma} > 0.7$, and from the jet by $\Delta R_{lj} > 0.5$. After the final selection the $ll\gamma$ cross section yields $\sigma_{Z\gamma} \times$ BR$(Z \to ll) = 1089 \pm 40$ (stat) $\pm$ 65 (syst) fb. With a $M_{ll\gamma}$ greater than 110 GeV applied to remove the FSR photon contribution, the cross section yields $\sigma_{Z\gamma} \times$ BR$(Z \to ll) = 288 \pm 15$ (stat) $\pm$ 11 (syst) fb. Both measurements are in agreement with the NLO SM prediction given by MCFM generator [5]. The unfolded differential cross section for

$Z\gamma \rightarrow ll\gamma$ production as a function of a photon p_T, $d(\sigma \times BR)/dp_T$, is shown in Fig. 3. The p_T spectra of photon candidates with $p_T > 30$ GeV shown in Fig. 4 were used to set the 95% C.L. limits on neutral ZZγ and Z$\gamma\gamma$ TGCs, and combined with previously published results in $ll\gamma$ [6] and $\nu\nu\gamma$ [7] final states. The combined one-dimensional 95% C.L. limits are $|h_{30}^{\gamma}| < 0.027$, $|h_{30}^{Z}| < 0.026$, $|h_{40}^{\gamma}| < 0.0014$ and $|h_{40}^{Z}| < 0.0013$ for $\Lambda = 1.5$ TeV. Imposing more stringent selection cuts on photon transverse energy $E_T^{\gamma} > 50$ GeV in $ll\gamma$ channel and $E_T^{\gamma} > 100$ GeV in $\nu\nu\gamma$ channel when analyzing 5 fb^{-1} of data, the CDF Collaboration sets the most stingent one-dimensional 95% C.L. limits on γ/ZZZ TGCs, -0.022 $< h_3^{\gamma} <$ 0.022, -0.020 $< h_3^{Z} <$ 0.021, $|h_4^{\gamma}| < 0.0008$ and $|h_4^{Z}| < 0.0009$ for $\Lambda = 1.5$ TeV [8].

2.3 $WZ \rightarrow l\nu ll$ Production

Selection of WZ events in $l\nu ll$ final states requires three highly energetic, isolated leptons and significant $\not\!\!E_T$. The CDF and DØ Collaborations analyzed 7.1 fb^{-1} [9] and 8.6 fb^{-1} [10] of integrated luminosity, respectively, in their WZ measurements. Even if these final states do not suffer from large backgrounds, a NeuroBayes neural network (NN) was used at CDF to further select signal from backgound and to extract the cross section by fitting the data to the shape of expected SM processes in the NN output distribution, shown in Fig. 5. The measured WZ cross section is $\sigma_{WZ} = 3.9\ ^{+0.8}_{-0.7}$(stat+syst) pb. The shape and normalization of Z p_T distribution are used to set the 95% C.L. limits on ZWW TGCs. The one-dimensional limits are -0.39 $< \Delta\kappa_Z <$ 0.90, -0.08 $< \Delta\lambda_Z <$ 0.10, and -0.08 $< \Delta g_1^Z <$ 0.20 for $\Lambda = 2.0$ TeV. The DØ Collaboration measures WZ cross section using the ratio of measured WZ to the inclusive Z cross sections, and the theoretical prediction for the production of the Z boson, both for $60 < M_{ll} < 120$ GeV, while fitting the M_T distribution shown in Fig. 6. This results in cancellation of the uncertainties due to lepton reconstruction and identification, and trigger efficiency measurement. The measured WZ cross section is $\sigma_{WZ} = 4.5\ ^{+0.6}_{-0.7}$ (stat+syst) pb.

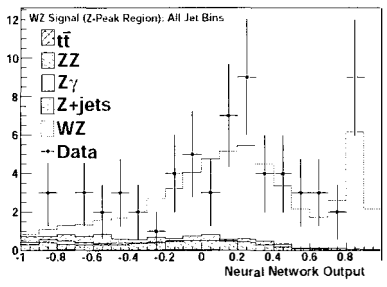

Figure 5: The NN output for $WZ \rightarrow l\nu ll$ signal, backgrounds and data collected by CDF.

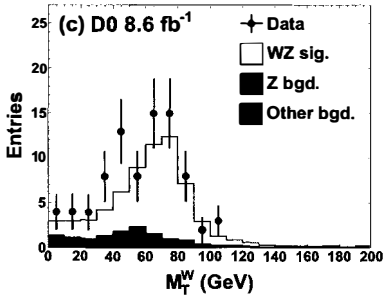

Figure 6: The transverse mass distribution for $WZ \rightarrow l\nu ll$ signal, backgrounds and data collected by DØ.

2.4 ZZ Production

CDF has studied ZZ production in $llll$ and $\nu\nu ll$ ($l = e, \mu$) final states using 6.1 fb^{-1} and 5.9 fb^{-1} of integrated luminosity [11], respectively. As the $\nu\nu ll$ final states suffer from large Drell-Yan background, a NeuroBayes NN was used to separate signal from backgound and to extract the cross section by fitting the data to the shape of expected SM processes in the NN output distribution, shown in Fig. 7. The combined ZZ cross section measured with $\nu\nu ll$ and $llll$ final states yields $\sigma_{ZZ} = 1.64\ ^{+0.44}_{-0.38}$ (stat+syst) pb. A new variable is built in the analysis of $\nu\nu ll$ final

states at DØ, effectively discriminating against Drell-Yan events. Its purpose is to minimize the mismeasurement of the transverse momentum of either the charged leptons or the hadronic recoil system which contributes to the reconstructed $\not\!\!E_T$. The NN output distributions shown in Fig. 8 were used to extract the ZZ cross section in the likelihood fit with the predicted number of ZZ events being allowed to float. The cross section measured in $\nu\nu ll$ final states and combined with previous result from $llll$ final states is $\sigma_{ZZ} = 1.44\ ^{+0.35}_{-0.34}$ (stat+syst) pb. Both CDF and DØ measurements are consistent with the NLO SM prediction.

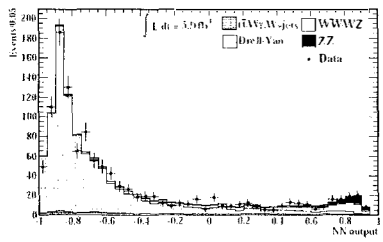

Figure 7: NN output distribution for the processes contributing to the $llvv$ sample, scaled to the best values of the fit to the CDF data.

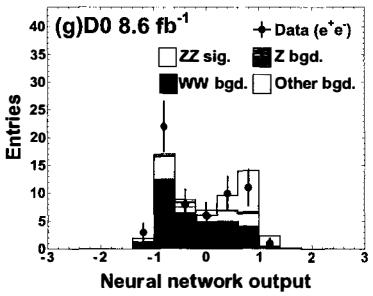

Figure 8: NN output distribution for the processes contributing to the $llvv$ sample, scaled to the best values of the fit to the DØ data.

2.5 $WW + WZ \rightarrow l\nu jj$ Production

Analyses of the $WW + WZ$ dijet final states have been performed at CDF and DØ applying b-tagging algorithms to maximize the separation between overlaping WZ and WW signals. The $l\nu jj$ ($l = e, \mu$) candidates, selected from 7.5 fb^{-1} of CDF data, are required to have a single isolated lepton with $p_T > 20$ GeV, significant $\not\!\!E_T$ and exactly two jets with $p_T > 20$ GeV. Events are divided into four categories based on lepton quality, detector coverage and number of b-tagged jets. The dijet mass distributions are used to extract the cross section by fitting to data using events with 1 and 2 b-tagged jets. The dijet mass distributions for events with 1 and 2 b-tagged jets are shown in Fig. 9. The combined cross section for WW and WZ production yields $\sigma_{WW+WZ} = 1.1\ ^{+0.3}_{-0.4} \times \sigma_{SM}$ (stat+syst) pb resulting in observed significance of 3σ [12]. The event selection at DØ requires a minimum of two jets with $p_T > 20$ GeV,

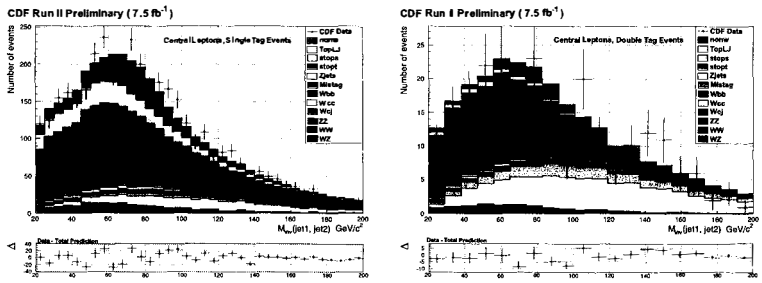

Figure 9: Invariant dijet mass distributions for 2 different event cathegories containing 1 (left) and 2 (right) b-tagged jets after the best MC fit to data.

and the electron (muon) with $p_T > 15$ (20) GeV, and significant $\not\!\!E_T$. Because of the large W+jets background contamination a Random Forest (RF) classifier is used to separate signal from background. The information on the number of b-tagged jets is used as an input to the RF. The signal cross section is determined from a fit of signal and background RF templates to the data with respect to variations in the systematic uncertainties and is measured to be $\sigma_{WW+WZ} = 19.6^{+3.2}_{-3.0}$ (stat+syst) pb with observed significance of 7.9σ (Fig. 10). Consistent results were obtained from the fit to the dijet mass distribution. The dijet mass peak in events with 0-tag jets, after background subtraction from data is shown in Fig. 11 compared to the MC prediction. When two signals, WW and WZ are treated separately in the fit of RF templates, the cross sections yield $\sigma_{WW} = 15.9^{+3.7}_{-3.2}$ (stat+syst) pb and $\sigma_{WZ} = 3.3^{+4.1}_{-3.3}$ (stat+syst) pb [13].

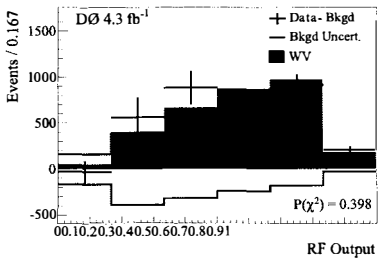

Figure 10: A comparison of the measured $WW + WZ$ signal to background-subtracted data in the RF output distribution (electron+muon, and 0, 1, and 2-tag sub-channels), after the combined fit to data using the RF output distributions.

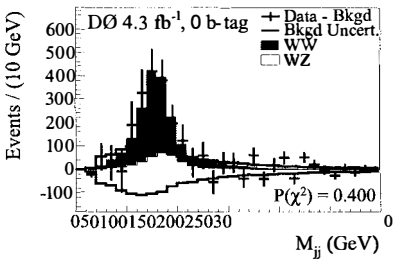

Figure 11: A comparison of the measured WW and WZ signals to background-subtracted data in the dijet mass distribution (electron+muon) for 0, 1, and 2-tag sub-channels after the combined fit to data using the dijet mass distribution.

2.6 $W/Z + Z \dashrightarrow b\bar{b}$ Production

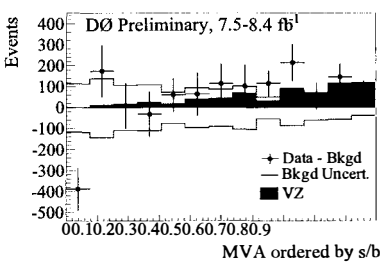

Figure 12: Comparison of measured $WZ + ZZ$ signal to background-subtracted data ordered in s/b at DØ.

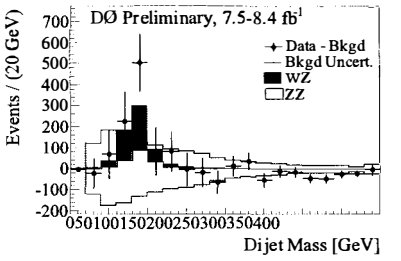

Figure 13: Comparison of measured WZ and ZZ signals to background-subtracted data in the dijet mass distribution for the sum of 1- and 2-tag sub-channels at DØ.

To validate the Tevatron low-mass SM Higgs boson search strategies, the Tavtron $H \dashrightarrow b\bar{b}$ searches ($WH \dashrightarrow l\nu b\bar{b}$, $ZH \dashrightarrow llb\bar{b}$ and $ZH \dashrightarrow \nu\nu b\bar{b}$) were adapted to measure the $WZ + ZZ$ cross section where Z boson decays into pair of heavy flavor jets, originating from c- and b-quarks. The event selection for the cross section measurement is the same as that used in the low mass Higgs analyses, described in [14,15,16,17,18,19]. Each collaboration combines the three final states to measure $WZ + ZZ$ cros section and finally, the measurement is performed combining

the six channels from both experiments. In these measurements only 1 and 2 b-tag sub-channels were used; the ratio of cross sections for WZ and ZZ productions is fixed by the SM while the WW cross section is constrained to its SM value, accounting for $\pm$ 7% theoretical uncertainty within which the WW rate is allowed to fluctuate. The final discriminant MC templates from individual final states were fit to data and yield the cross section of $\sigma_{WZ+ZZ} = (1.6 \pm 0.8) \times \sigma_{SM}$ in DØ $l\nu bb$ final states [14], $\sigma_{WZ+ZZ} = (0.1 \pm 0.6) \times \sigma_{SM}$ in DØ $llbb$ final states [16], and $\sigma_{WZ+ZZ} = (1.5 \pm 0.5) \times \sigma_{SM}$ in DØ $\nu\nu bb$ final states [18].

The combined cross section measurement at DØ yields $\sigma_{WZ+ZZ} = (1.13 \pm 0.36) \times \sigma_{SM}$ with observed significance of 3.3 σ [20]. The final discriminant with bins of individual discriminants have been ordered in s/b is shown in Fig. 12. The dijet mass peak in 1-tag and 2-tag sub-channels combined, after background subtraction from data is shown in Fig. 13 compared to the MC prediction. Similar distributions for CDF combined $WZ + ZZ$ cross section measurement are shown in Fig. 14 and Fig. 15. The combined cross section measurement at CDF yields $\sigma_{WZ+ZZ} = 4.1^{+1.4}_{-1.3}$ (stat+syst) pb with observed significance of 3.2 σ. The combination of

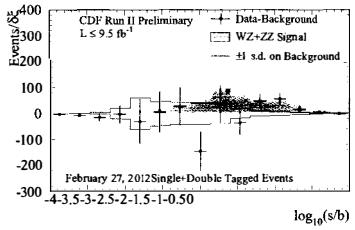

Figure 14: Comparison of the measured $WZ + ZZ$ signal to background-subtracted data ordered in s/b at CDF.

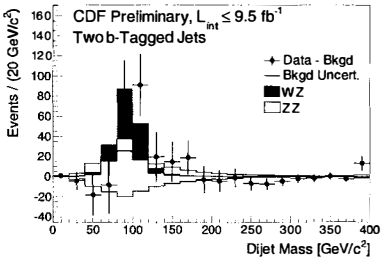

Figure 15: Comparison of the measured WZ and ZZ signals to background-subtracted data in the dijet mass distribution for the 2-tag sub-channel at CDF.

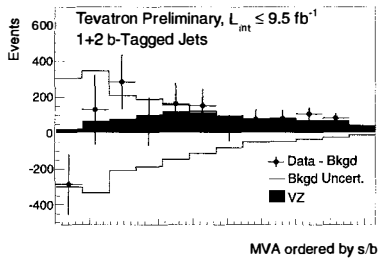

Figure 16: Comparison of the DØ+CDF measured $WZ + ZZ$ signal to background-subtracted data ordered in s/b.

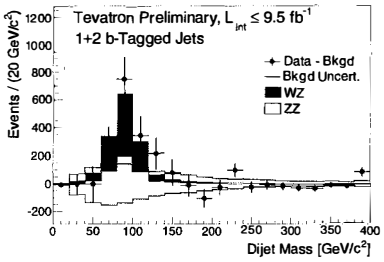

Figure 17: Comparison of the DØ+CDF measured WZ and ZZ signals to background-subtracted data in the dijet mass distribution for the 2-tag sub-channel.

six individual CDF and DØ final discriminants yields a $WZ + ZZ$ cross section of $\sigma_{WZ+ZZ} = 4.47 \pm 0.64^{+0.73}_{-0.72}$ (stat+syst) pb with an observed significance of 4.6 σ. The final discriminant with bins of individual discriminants ordered in s/b and the dijet mass peak in 1-tag and 2-tag sub-channels combined, after background subtraction from data are shown in Fig. 16 and Fig. 17, respectively.

3 Summary

The CDF and DØ Collaborations have presented recent results of diboson production studies using the data collected at the Tevatron between 2002 - 2011. Measured cross sections and TGCs are in agreement with the SM predictions. We also present the first evidence for the production of $WZ + ZZ$ with heavy flavor jets in final states, separately achived by each Tevatron experiment and combined. This clearly demonstrates the ability of the CDF and DØ Collaborations to measure a cross sections of the same order of magnitude as that expected for Higgs boson production in association with a vector boson at the Tevatron and validates the background modeling and analysis techniques used in the Tevatron low-mass Higgs boson searches.

References

1. K. Hagiwara, J. Woodside and D. Zeppenfeld, *Phys. Rev.* D **41**, 2113 (1990).
2. DØ uses a spherical coordinate system with the z axis running along the proton beam axis. The angles θ and ϕ are the polar and azimuthal angles, respectively. Pseudorapidity is defined as $\eta = -\ln[\tan(\theta/2)]$, in which θ is measured with respect to the proton beam direction.
3. V. M. Abazov *et al* (DØ Collaboration), *Phys. Rev. Lett.* **107**, 241803 (2011).
4. V. M. Abazov *et al* (DØ Collaboration), *Phys. Rev.* D **85**, 052001 (2012).
5. J. Campbell, R. Ellis and C. Williams, *J. High Energy Phys.* **07**, 018 (2011).
6. V. M. Abazov *et al* (DØ Collaboration), *Phys. Rev. Lett.* **100**, 131801 (2008).
7. V. M. Abazov *et al* (DØ Collaboration), *Phys. Rev. Lett.* **102**, 201802 (2009).
8. T. Aaltonen *et al* (CDF Collaboration), *Phys. Rev. Lett.* **107**, 051802 (2011).
9. T. Aaltonen *et al* (CDF Collaboration), arXiv:1202.6629 [hep-ex].
10. T. Aaltonen *et al* (CDF Collaboration), arXiv:1201.5652 [hep-ex].
11. T. Aaltonen *et al* (CDF Collaboration), *Phys. Rev. Lett.* **108**, 101801 (2012).
12. T. Aaltonen *et al* (CDF Collaboration), CDF Note 10598 (2011).
13. V. M. Abazov *et al* (DØ Collaboration), *Phys. Rev. Lett.* **108**, 181803 (2012).
14. V. M. Abazov *et al* (DØ Collaboration), DØ Note 6220-CONF (2011).
15. T. Aaltonen *et al* (CDF Collaboration), CDF Note 10796 (2012).
16. V. M. Abazov *et al* (DØ Collaboration), DØ Note 6256-CONF (2011).
17. T. Aaltonen *et al* (CDF Collaboration), CDF Note 10799 (2012).
18. V. M. Abazov *et al* (DØ Collaboration), DØ Note 6223-CONF (2011).
19. T. Aaltonen *et al* (CDF Collaboration), CDF Note 10798 (2012).
20. V. M. Abazov *et al* (DØ Collaboration), arXiv:1204.4496 [hep-ex].
21. The CDF and DØ Collaborations, arXiv:1203.3782 [hep-ex].